
Unsupervised/Semi-supervised Deep Learning for Low-dose CT Enhancement

Mingrui Geng*
Xian Jiaotong University

Yun Deng
Xian Jiaotong University

Qian Zhao
Xian Jiaotong University

Qi Xie
Xian Jiaotong University

Dong Zeng
Southern Medical University

Jianhua Ma
Southern Medical University

Wangmeng Zuo
Harbin Institute of Technology, China

Deyu Meng[†]
Xian Jiaotong University

Abstract

Recently, deep learning (DL) methods have been proposed for the low-dose computed tomography (LdCT) enhancement, and obtain good trade-off between computational efficiency and image quality. Most of them need to pre-collect large number of ground-truth/high-dose sinograms with less noise, and train the network in a supervised end-to-end manner. This may bring major limitations on these methods because the number of such low-dose/high-dose training sinogram pairs would affect the network's capability and sometimes the ground-truth sinograms are hard to be obtained in large scale. Since large number of low-dose ones are relatively easy to obtain, it should be critical to make these sources play roles in network training in an unsupervised learning manner. To address this issue, we propose an unsupervised DL method for LdCT enhancement that incorporates unlabeled LdCT sinograms directly into the network training. The proposed method effectively considers the structure characteristics and noise distribution in the measured LdCT sinogram, and then learns the proper gradient of the LdCT sinogram in a pure unsupervised manner. Similar to the labeled ground-truth, the gradient information in the unlabeled LdCT sinogram can be used for sufficient network training. The experiments on the patient data show effectiveness of the proposed method.

1 Introduction

Computed tomography (CT) has been widely used for clinical diagnosis. Meanwhile, concerns regarding radiation-related cancer in CT examination are growing, especially in the repeated CT scans [2]. Therefore, decreasing X-ray dose to reduce risk to patients is highly desired. However, this would lead to severe noise-induced artifacts in the filtered backprojection (FBP) reconstructed image without adequate treatments [7][13][22].

Many methods have been proposed to enhance the LdCT image quality. These methods can be mainly divided into two strategies. One is to characterize noise distribution or designate somewhat handcrafted prior based on the conventional maximum a posteriori probability (MAP) model [14][15][19][21]. Although these MAP-based methods can yield high-quality LdCT sinograms to some extent, they may have intrinsic limitations: First, the iterative solution process of these methods yields a high computational cost, and can be hundreds of times slower than DL methods in prediction process. Second, these methods process each sinogram separately, and thus are not able to integrate all CT sinogram sources to extract their common latent knowledge underlying desired CT sinograms.

*Mingrui Geng and Yun Deng made equal contributions to this work.

[†]Deyu Meng is the corresponding author. Email: dymeng@mail.xjtu.edu.cn.

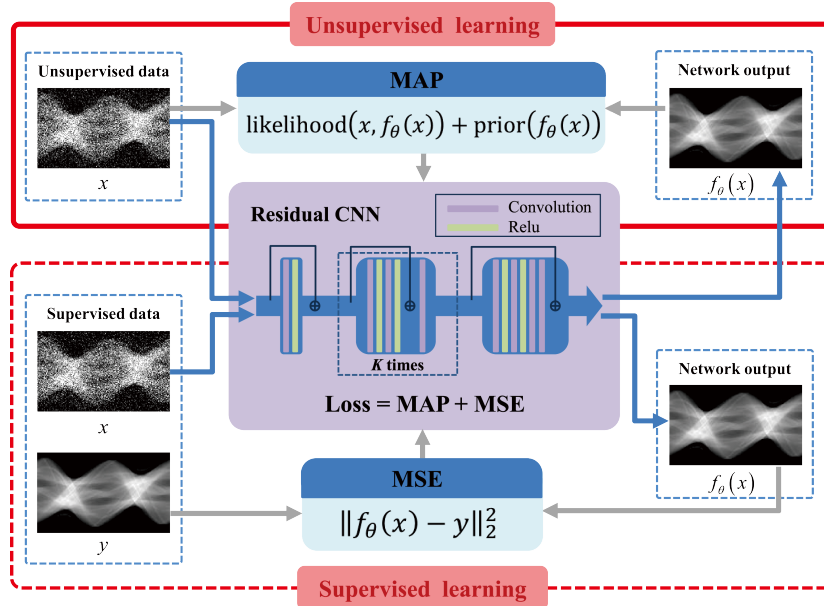


Figure 1: The framework of the proposed method. The unsupervised part (solid line) is trained directly on low-dose CTs, where the MAP model will guide the right gradients for network training. The supervised part (dashed line) is guided by the supervised low-dose/high-dose CT pairs, in traditional DL training manner. These two parts can be combined to form a semi-supervised DL framework.

The other is deep learning (DL) approach, which learns the mapping from the LdCT images to high-dose ones in an end-to-end manner [3][4][8][17], and has obtained state-of-the-art performance on the task. However, this line of methods needs to pre-collect a large quantity of low-dose/high-dose CT image pairs as the training inputs/outputs of the network, where the labeled LdCT images are usually generated from the high-dose images via simulation methods. However, due to the limitations of privacy, collecting costs and domain biases, it is always impractical to attain sufficient training sample pairs as expected. Moreover, the current CT image enhancement methods based on DL do not take good advantage of abundant information in the unlabeled CT dataset.

It thus has become a critical issue to make unsupervised LdCT images, without guidance of the corresponding high-dose ones, capable of being sufficiently involved in deep network training. Such an unsupervised deep learning issue actually has been attracting increasing attention throughout machine learning [11], pattern recognition [12], computer vision [26], and many other related domains.

Against the aforementioned issue, this work presents an unsupervised DL regime for directly involving unlabeled LdCT sinograms, without requirement of their high-dose ones, into network training. Specifically, through fully exploring both the structure characteristics underlying a clean CT sinogram and specific noise configuration in a measured LdCT sinogram, we can use a MAP objective to fully represent both of these knowledge contained in LdCT sinograms by elaborately designed regularization and likelihood terms, respectively. Such a MAP model facilitates an effective exploration on the gradient direction along which the input LdCT sinogram should be oriented to the expected clean one, and thus can be readily employed into the network training. Such an unsupervised DL regime can also be easily integrated with supervised CT sinogram pairs to further ameliorate the performance of the method. The basic implementation mechanism of the method is illustrated in Fig. 1.

In summary, this paper mainly makes the following contributions:

- (1) Towards the low-dose CT enhancement issue, this work first proposes a feasible unsupervised DL regime, without need of supervised low-dose/high-dose CT sinogram pairs as inputs/outputs of the network, while directly being implemented on unsupervised LdCT sinograms. This method facilitates a sufficient utilization of unlabeled LdCT sinograms, and makes the DL strategy capable of being more easily and generally implemented in real scenarios with few high-dose data sources.
- (2) We further extend our unsupervised DL method to semi-supervised version. For supervised data, we construct the objective function in the data-driven manner according to its supervised information.

For unsupervised data, we construct the objective function in the model-driven manner by fully considering its prior structure and noise configuration. Such supervised and unsupervised integration is also inspiring to construct more general semi-supervised DL paradigms for other tasks.

(3) We have verified the superiority of the proposed unsupervised/semi-supervised DL strategy on real LdCT sinograms, in terms of both computational speed and accuracy, as compared with the traditional methods.

This paper is organized as follows: Section 2 introduces some related works on the investigated task. Section 3 presents our basic models and algorithms. Section 4 demonstrates the experimental results and finally we give the conclusion in Section 5.

2 Related Work

2.1 Traditional Low-dose CT enhancement approaches

Traditional methods can be mainly categorized into two classes, sinogram statistical iterative methods, which only use the information in sinogram domain, and model-based iterative reconstruction (MBIR) methods, which combine the information of sinogram domain and CT image domain.

The penalized weighted least-square (PWLS) method is the representative work on the first class. One typical PWLS method was proposed by Wang et al. [19], who modeled accurate noise distribution and imposed a proper regularization to reduce sinogram noise. Moreover, Xie et al. [21] proposed a method taking full use of both the statistical properties of projection data and prior structure knowledge under sinogram domain for CT denoising and reached the state-of-the-art in this kind of methods. Comparatively, MBIR methods can offer the potential to reconstruct CT image with better bias-variance performance by using prior information of CT image domain. Some works explored different prior information in recovery model, such as total variation(TV) and its variants [1][18][29], dictionary learning [23] and nonlocal means [5].

Though some of these methods show satisfactory effects on certain LdCT images, they can only be implemented on each CT image separately, while cannot get a deterministic prediction function to directly input LdCT images and output expected clean ones. This makes them always very time-consuming in real scenarios. Besides, such methods can only make use of one CT image to explore its latent ground-truth one, while cannot integrate more CT images to summarize its insightful statistical common knowledge and serve such useful knowledge for further LdCT enhancement. DL techniques thus attract more attention recently by finely ameliorating these issues.

2.2 Deep learning approaches

Currently, the data-based DL approaches has achieved inspiring achievements to this issue. For example, Chen et al. [4] first introduced CNN in CT images denoising task. To extract features more efficiently, he further used a encoder-decoder network instead [3]. After that, Yang et al. [24] introduced the perceptual loss in CT enhancement task, which measured the difference between low-dose/high-dose CT image pairs in a high-level feature space to make them look more similar. Further, in order to preserve the detail information as well, Yi et al. [25] combined the GAN and a low-level feature space measurement network named sharpness detection network, to decrease the blur effect.

Though DL methods have an exciting performance and fast processing speed, they seriously rely on the pre-collected LdCTs and corresponding high-dose ones as their ground-truth. Such supervised samples, however, are always very hard to get and need take large costs including human labor and collecting time. Besides, the collection of high-dose CT images will always cause great harm to the patients' health. It is thus highly expected to have an unsupervised DL paradigm, by only inputting LdCTs into network for training without need of their guided high-dose ones.

3 Unsupervised/Semi-supervised Deep Learning for LdCT Enhancement

3.1 Data-based supervised deep learning

Let $x_i \in \mathbb{R}^m$, $i = 1, 2, \dots, n$ be the LdCT sinogram and $y_i \in \mathbb{R}^m$ be the corresponding high-dose sinogram, f_θ is the mapping $f_\theta: x \rightarrow \tilde{y}$, where \tilde{y} is the predicted output by CNN. We thus denote \tilde{y} as $f_\theta(x)$, where θ is the parameters of CNN mapping. In the DL network for CT image enhancement,

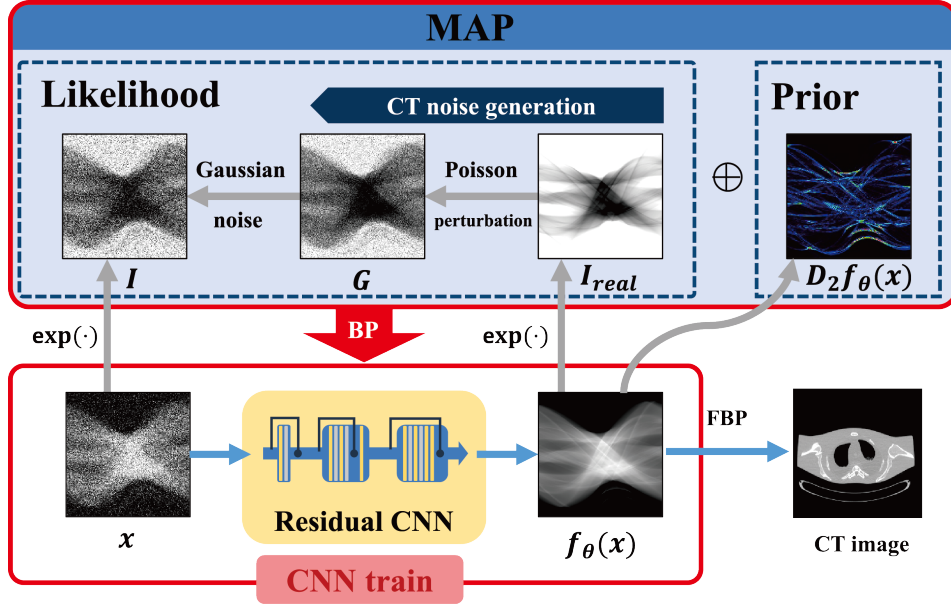


Figure 2: Illustration of the MAP model construction.

training dataset is a set of input-target pairs $\{x_i, y_i\}_{i=1, \dots, n}$. A commonly utilized strategy is to minimize the following mean square error (MSE) for network parameter tuning:

$$\min_{\theta} \sum_i L(f_{\theta}(x_i), y_i) = \min_{\theta} \sum_i \|f_{\theta}(x_i) - y_i\|_2^2. \quad (1)$$

The supervised DL model can achieve a good trade-off between image quality and computational efficiency under adequately corrected supervised CT sinogram pairs. However, the number of the supervised sinograms would affect the network’s capability and sometimes the ground-truth sinograms are difficult to obtain. Instead, the unlabeled LdCT sinograms can be relatively easily collected. Therefore, the unlabeled LdCT dataset is expected to be also used in the network training to further improve enhancement performance.

3.2 Model-based unsupervised deep learning

We first shortly introduce the basic generation process of a CT image. I_0 denotes the number of unattenuated photons (X-ray fluence), I is the number of the attenuated photons arriving at the detector and usually follows the combined Poisson-Gaussian noise distribution. Specifically, based on [21], G represents the attenuated photons with additive electronic noise only, ignoring the quanta fluctuation of X-ray interactions theoretically. And I_{real} denotes the attenuated photons without any noise, which can be considered as the desired projection data. CT sinogram can be generated by I after a logarithmic transformation. The final CT image can be got by FBP. The overall generation process is illustrated in Fig. 2.

We then introduce how to express the statistical properties (leading to noises), as well as its expected recovery structures, underlying a LdCT sinogram. This knowledge is then used to achieve a proper gradient direction to feed into the network and make the input LdCT sinogram orient to the expected clean ones as well as remove the unexpected noise.

The projection data I are generally mixed with noise and can be expressed as follows:

$$I = G + \varepsilon, \quad (2)$$

where $\varepsilon \in \mathbb{R}^N$ denotes the electronic noise. For projection I , the first term follows X-ray photon statistics and the second term leads to electronic noise background [16][22]. The electronic noise ε can be described as a simple Gaussian distribution [14]: $\varepsilon_j \sim \mathcal{N}(\varepsilon_j|0, \sigma^2)$, where σ^2 denotes the variance of noise. Based on [14] we can obtain that

$$p(I|G) = \frac{1}{(2\pi)^{N/2} \sigma^N} \exp^{-\frac{\|I-G\|_2^2}{2\sigma^2}}. \quad (3)$$

The received quanta G can be well depicted by the compound Poisson distribution [10] [21] as follows:

$$p(G|f_\theta(x)) = \prod_{j=1}^N \left(\frac{(I_{0j}e^{-f_\theta(x)_j})^{G_j}}{G_j!} \exp(-I_{0j}e^{-f_\theta(x)_j}) \right), \quad (4)$$

where I_{0j} denotes I_0 along the projection path j . x and $f_\theta(x)$ denote the log-transformations of I and I_{real} , corresponding to the input LdCT sinogram and ideal output one of the network, respectively, with elements $(x)_j$ and $f_\theta(x)_j$, where N is the total number of measurements in the scan. By combining (3) and (4), the generative-model of projection data can be obtained as [21]:

$$p(I, G|f_\theta(x)) = \prod_{j=1}^N \left(\frac{(I_{0j}e^{-f_\theta(x)_j})^{G_j}}{G_j!} \exp(-I_{0j}e^{-f_\theta(x)_j}) \right) \frac{1}{(2\pi)^{N/2}\sigma^N} \exp^{-\frac{\|I-G\|_2^2}{2\sigma^2}}. \quad (5)$$

Note that the electronic noise background and the statistical property of photon statistics have been considered in (3) and (4). Besides the above understanding on the statistical properties on LdCT sinogram, constituting the likelihood term in the optimized MAP model, we can also get useful prior knowledge on the ideal recovery, to further compensate the model.

Based on [21], the sinogram data is formed as a manifold approximately constituted by a combination of several flat surface. This flats-combination prior can be introduced to describe the properties of the sinogram, i.e., sparsity in its second order derivative, which can be formulated as:

$$p(f_\theta(x)) \propto e^{-k\|\ln(D_2f_\theta(x)+\varepsilon)-\ln(\varepsilon)\|_1}, \quad (6)$$

where k is a constant parameter, and D_2 is the second order difference matrix. This class of distribution can encode the transformed-sparsity of data.

By combining (5) and (6), the complete posterior distribution on data can be formulated as follows:

$$\begin{aligned} p(G, f_\theta(x)|I) &= \frac{p(I, G|f_\theta(x))p(f_\theta(x))}{p(I)} \\ &\propto \exp\left(-\frac{\|I-G\|_2^2}{2\sigma^2} - k\|\ln(D_2f_\theta(x)+\varepsilon)-\ln(\varepsilon)\|_1\right) \prod_{j=1}^N \left(\frac{(I_{0j}e^{-f_\theta(x)_j})^{G_j}}{G_j!} \right). \end{aligned} \quad (7)$$

The ideal $f_\theta(x)$ can be estimated under MAP framework [6][10][14]. The network can then be trained under the guidance of the following loss term in an unsupervised DL manner:

$$\begin{aligned} \arg \min_{\theta, G} \sum_i \sum_{j=1}^N \left(\frac{\|I-G\|_2^2}{2\sigma^2} - G_j \ln(I_{0j}) + G_j f_\theta(x)_j + \ln(G_j!) + I_{0j}e^{f_\theta(x)_j} \right) \\ + k \sum_i \|\ln(D_2f_\theta(x_i) + \varepsilon) - \ln(\varepsilon)\|_1. \end{aligned} \quad (8)$$

3.3 Semi-supervised deep learning

We can then naturally construct semi-supervised DL scheme to fully utilize both supervised and unsupervised LdCT data sources, via combining the aforementioned two types of models. The corresponding loss function can be expressed as follows:

$$\begin{aligned} L(G, \theta) &= \sum_{x_i \in C_1} \left(\sum_j \left(\frac{\|I-G\|_2^2}{2\sigma^2} - G_j (\ln I_{0j}) + G_j f_\theta(x_i)_j + \ln G_j! + I_{0j}e^{-f_\theta(x_i)_j} \right) \right. \\ &\quad \left. + k\|\ln(D_2f_\theta(x_i) + \varepsilon) - \ln(\varepsilon)\|_1 \right) + \lambda \sum_{x_i \in C_2} \|f_\theta(x_i) - y_i\|_2^2, \end{aligned} \quad (9)$$

where C_1 and C_2 are the sets of unsupervised and supervised sinogram data, respectively. λ is the trade-off parameter, which balances the loss functions of supervised and unsupervised learning components. The value of this parameter can be set based on the portions of two parts of data. The more we have the supervised ones, the larger it should be set.

By using such loss setting, the network can be trained both on supervised and purely unsupervised inputs. Note that when $\lambda = 0$, this model will directly degenerate to the unsupervised one.

Algorithm 1 Algorithm for Update G

Input: x_i, I, I_0 and σ **Output:** G

- 1: Initialize G as the value of G we obtained in the last step of complete algorithm
 - 2: **for** $j = 1 : N$ **do**
 - 3: **while** $h(G_j) > h(G_j + 1)$ **do**
 - 4: Update $G_j = G_j + 1$
 - 5: **end while**
 - 6: **while** $h(G_j) > h(G_j - 1)$ **do**
 - 7: Update $G_j = G_j - 1$
 - 8: **end while**
 - 9: **end for**
-

Algorithm 2 Algorithm for Solving (9)

Input: $I_0, I = I_0 \odot e^{-x_i}$ **Output:** the denoised scan $f_\theta(x)$

- 1: Initialize CNN parameter θ
 - 2: **while** not convergence **do**
 - 3: Update G by Algorithm 1.
 - 4: Update θ by Back Propagation Algorithm.
 - 5: **end while**
-

3.4 Alternative optimization algorithm for solving the model

We can readily employ the alternative optimization algorithm to calculate (9). The optimization procedures can be summarized as follows:

With the other parameters fixed, G can be updated by solving $\arg \min_G L(G, \theta)$, that is:

$$\arg \min_G \sum_j \left(\frac{\|I - G\|_2^2}{2\sigma^2} - G_j (\ln I_{0j}) + G_j f_\theta(x_i)_j + \ln G_j! \right). \quad (10)$$

This problem can be further separated for each G_j as:

$$\arg \min_G h(G_j) = \frac{\|I - G\|_2^2}{2\sigma^2} - G_j (\ln I_{0j}) + G_j f_\theta(x_i)_j + \ln G_j!, \quad (11)$$

whose solution can be obtained by Algorithm 1.

With the other parameters fixed, θ can be updated by solving $\arg \min_\theta L(G, \theta)$, which is equivalent to the following problem:

$$\begin{aligned} \arg \min_\theta \sum_{x_i \in C_1} \left(\sum_j \left(G_j f_\theta(x_i)_j + I_{0j} e^{-f_\theta(x_i)_j} \right) + k \| \ln(D_2 f_\theta(x_i) + \varepsilon) - \ln(\varepsilon) \|_1 \right) \\ + \lambda \sum_{x_i \in C_2} \| f_\theta(x_i) - y_i \|_2^2. \end{aligned} \quad (12)$$

This corresponds to a standard network training problem, and can be easily calculated by calling any of current deep learning algorithms, like Adam [9], for network parameter tuning.

The whole procedure for optimization of (9) can be summarized in Algorithm 2.

4 Experimental results

The performance of the proposed two methods, i.e., unsupervised learning (unsup-CNN) and semi-supervised learning (semi-CNN), is verified in this section. Comparison methods include PWLS [19], MAP-FC [21], and supervised CNN methods. The PSNR, SSIM [20] and FSIM [28] are used for performance evaluation. In addition, the running time of all algorithms are demonstrated for speed comparison. The "2016 Low-dose CT Grand Challenge datasets"³ were used in the experiments. The

³ <https://www.aapm.org/GrandChallenge/LowDoseCT>

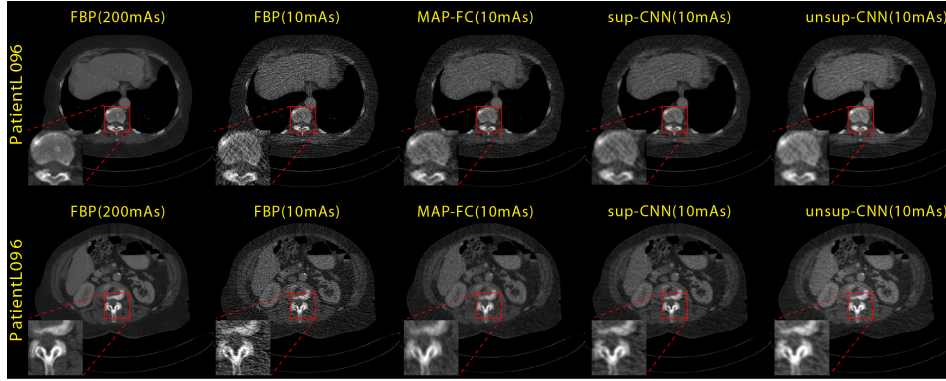


Figure 3: The high-dose sinogram (200 mAs) and low-dose images processed by the FBP, MAP-FC, sup-CNN and unsup-CNN methods. All the images are displayed in the same window.

Table 1: Quantitative measurements of results of all competing methods at three different noise levels.

Patient	dose	L096			L096			Time
		PSNR	SSIM	FSIM	PSNR	SSIM	FSIM	
10mAs	FBP	29.2551	0.6157	0.8916	33.2117	0.7662	0.9274	-
	MAP-FC	35.3356	0.8465	0.9461	38.9901	0.9224	0.9681	21.76
	sup-CNN	36.8963	0.9128	0.9658	39.1643	0.9494	0.9738	0.083
	unsup-CNN	35.5475	0.9128	0.9629	40.1458	0.9471	0.9745	0.083
12.5mAs	FBP	30.4716	0.6799	0.9178	34.5637	0.8111	0.9444	-
	MAP-FC	36.5699	0.8786	0.9602	39.9781	0.9376	0.9762	21.76
	sup-CNN	37.6384	0.9244	0.9725	40.0542	0.9622	0.9823	0.083
	unsup-CNN	36.1274	0.9338	0.9974	40.3582	0.9475	0.9803	0.083
20mAs	FBP	33.6759	0.7887	0.9521	37.3508	0.8851	0.9682	-
	MAP-FC	38.7972	0.9229	0.9771	41.7376	0.9593	0.9841	21.76
	sup-CNN	38.8859	0.9406	0.9812	42.1377	0.9593	0.9855	0.083
	unsup-CNN	38.3038	0.9439	0.9813	41.3767	0.9593	0.9846	0.083

normal-dose CT data were acquired with 120 kVp and 200 effective mAs. LdCT data at three dose levels, 20 mAs, 12.5 mAs and 10 mAs, were generated via the simulation method [27]. The high-dose ones at 200 mAs are considered as the ground-truth for comparison in the experiments. More detailed information on the utilized network settings can be referred to in supplementary material.

4.1 On the effect of unsupervised DL method

To verify the effectiveness of the unsupervised CNN (unsup-CNN) method, supervised CNN (sup-CNN) method and MAP-FC method were conducted for comparison. For unsupervised CNN, we only used 50 LdCT sinograms as training set. For sup-CNN method, we used 50 low-dose/high-dose CT sinogram pairs as training set.

Fig. 3 shows the corresponding results processed by the different methods. It can be observed that MAP-FC, sup-CNN and unsup-CNN can suppress noises effectively. Because the bone regions contain abundant structures details, two regions indicated by the red boxes are selected to validate image quality improvement. It is seen that the unsup-CNN method preserves more details with higher resolution in the magnified ROI than the other competing methods. In addition, Table 1 lists the PSNR, FSIM and SSIM measurements and running time of all competing methods. It is seen that the two CNN-based methods perform better than the MAP-FC method in all cases. And the unsup-CNN method can obtain similar performance to the sup-CNN method, while the latter require extra supervised samples for training. These results substantiate that the proposed unsup-CNN method can properly extract gradients to guide network training on purely unsupervised LdCT sinograms.

4.2 On the effect of unsupervised DL method for single image

To evaluate the capability of the unsupervised network in extreme cases, only one LdCT sinogram was used for network training. Fig. 4 shows the CT images processed by the FBP, PWLS, MAP-FC

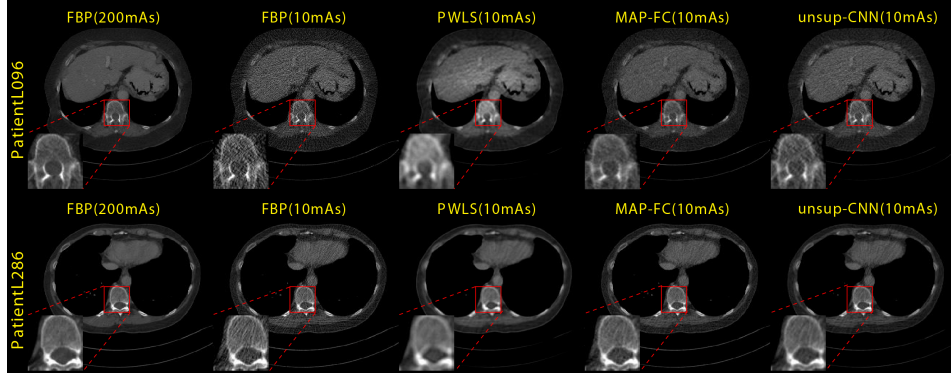


Figure 4: The high-dose sinogram (200 mAs) and low-dose sinogram measurements processed by the FBP, PWLS, MAP-FC, sup-CNN and unsup-CNN methods. All the images are displayed in the same window.

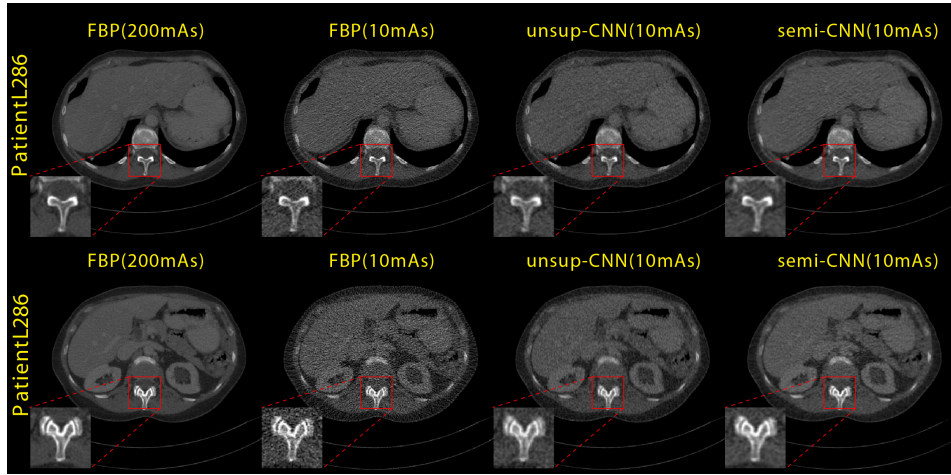


Figure 5: The high-dose sinogram (200 mAs) and low-dose sinogram measurements processed by the FBP, sup-CNN and semi-CNN methods. All the images are displayed in the same window.

and unsup-CNN methods. Through visual inspection, it is seen that the PWLS and MAP-FC can suppress noise-induced artifacts well at the cost of resolution loss. The proposed unsup-CNN method effectively reduces the noise-induced artifacts and also preserves the resolution successfully.

This experiment illustrates that the proposed unsup-CNN can also work well even the training data is limited. This is attributed to that network can also work as an optimizer to minimize the target function. Note that in such scenarios, one superiority of the proposed method is that it can get a explicit prediction network, which can be efficiently utilized for further CT enhancement task.

4.3 On the effect of semi-supervised DL method

We used 20 low-dose/high-dose CT sinogram pairs (supervised samples) and 50 LdCT sinograms (unsupervised samples) as training data in the semi-supervised CNN experiment. For comparison, we used the same LdCT data as training data in the unsupervised CNN network. Fig. 5 shows the LdCT results processed by the FBP, unsup-CNN and semi-CNN methods. It is evident that both of the proposed CNN-based methods are able to remove noise-induced artifacts satisfactorily compared to the high-dose (200 mAs) one. The semi-CNN method performs better than the unsup-CNN method in the noise-induced artifacts in the flat region. The zoomed bone regions (ROIs indicated by the red boxes) suggests that the proposed semi-CNN method can reconstruct the fine structures with higher resolution than the unsup-CNN method.

Table 2 lists the PSNR, FSIM, and SSIM measurements for the results with the FBP, unsup-CNN and semi-CNN methods at three noise levels. Both the CNN-based methods outperform the conventional

Table 2: The quantitative measurements of the results with the different methods at three noise levels.

Patient dose		L286			L286		
		PSNR	SSIM	FSIM	PSNR	SSIM	FSIM
10mAs	FBP	29.9772	0.6426	0.8857	29.8674	0.6275	0.8757
	unsup-CNN	36.6898	0.9053	0.9514	36.7192	0.9048	0.9515
	semi-CNN	37.4342	0.9165	0.9604	37.6782	0.9569	0.9592
12.5mAs	FBP	31.4157	0.7042	0.9137	31.2056	0.6875	0.9002
	unsup-CNN	37.0445	0.9191	0.9649	36.9405	0.9224	0.9599
	semi-CNN	38.2185	0.9128	0.9681	38.2185	0.9213	0.9637
20mAs	FBP	34.3839	0.8088	0.9593	34.0601	0.7967	0.9401
	unsup-CNN	38.4932	0.9384	0.9699	38.3164	0.9352	0.9378
	semi-CNN	39.6660	0.9406	0.9776	39.5755	0.9457	0.9751

FBP method. The semi-CNN method that combinationally uses the supervised and unsupervised CT data sources leads to its better reconstruction quality than the unsup-CNN methods.

5 Conclusion

In this study, we have proposed a new mechanism on making DL performable on unsupervised training data, and especially realized it for the task of LdCT enhancement. Through sufficiently understanding and formulating the statistics properties embedded in data and prior structures underlying the expected recovery data, we can construct a MAP model, which facilitates an effective gradient direction to guide the unsupervised LdCT transformed to the expected clean one. Such gradients can easily feed into the network for its parameter tuning, and thus the deep learning can be implemented in an unsupervised manner. The proposed method constitutes a general paradigm to realize unsupervised/semi-supervised DL for more related tasks, like signal recovery and image reconstruction.

References

- [1] C. Bouman and K. Sauer. *A generalized Gaussian image model for edge-preserving MAP estimation*, volume 2. IEEE Transactions on Image Processing, 1993.
- [2] D Brenner. Mo-fg-207a-02: What do we really know about cancer risks at doses pertinent to ct scans. *Medical Physics*, 43(6):3714, 2016.
- [3] H. Chen, Y. Zhang, M. K. Kalra, F. Lin, Y. Chen, P. Liao, J. Zhou, and G. Wang. Low-dose ct with a residual encoder-decoder convolutional neural network. *IEEE Transactions on Medical Imaging*, 36(12):2524–2535, 2017.
- [4] H Chen, Y Zhang, W Zhang, P Liao, K Li, J Zhou, and G Wang. Low-dose ct via deep neural network. *Biomedical Optics Express*, 8(2):679–694, 2016.
- [5] Y Chen, D Gao, C Nie, L Luo, W Chen, X Yin, and Y Lin. Bayesian statistical reconstruction for low-dose x-ray computed tomography using an adaptive-weighting nonlocal prior. *Computerized Medical Imaging & Graphics*, 33(7):495, 2009.
- [6] J Fessler. Statistical image reconstruction methods for transmission tomography. In *Handbook of Medical Imaging, Volume 2. Medical Image Processing and Analysis*, 2000.
- [7] J Hsieh. Adaptive streak artifact reduction in computed tomography resulting from excessive x-ray photon noise. *Medical Physics*, 25(11):2139–2147, 1998.
- [8] E Kang, J Min, and J Ye. A deep convolutional neural network using directional wavelets for low-dose x-ray ct reconstruction. *Medical Physics*, 44(10):e360–e375, 2017.
- [9] Diederik P Kingma and Jimmy Ba. Adam: A method for stochastic optimization. *Proceedings of the 3rd International Conference on Learning Representations (ICLR)*, 2014.
- [10] P. J. La Rivière, J. Bian, and P. A. Vargas. Penalized-likelihood sinogram restoration for computed tomography. *IEEE Transactions on Medical Imaging*, 25(8):1022–1036, 2006.

- [11] J Lehtinen, J Munkberg, J Hasselgren, S Laine, T Karras, M Aittala, and T Aila. Noise2noise: Learning image restoration without clean data. *arxiv*, 2018.
- [12] W Lotter, G Kreiman, and D Cox. Deep predictive coding networks for video prediction and unsupervised learning. 2016.
- [13] H Lu, I Hsiao, X Li, and Z Liang. Noise properties of low-dose ct projections and noise treatment by scale transformations. In *IEEE Nuclear Science Symposium Conference Record*, pages 1662–1666, 2001.
- [14] J Ma, H Zhang, Y Gao, J Huang, Z Liang, Q Feng, and W Chen. Iterative image reconstruction for cerebral perfusion ct using pre-contrast scan induced edge-preserving prior. *Physics in Medicine & Biology*, 57(22):7519–7542, 2012.
- [15] L Ouyang, T Solberg, and J Wang. Effects of the penalty on the penalized weighted least-squares image reconstruction for low-dose cbct. *Physics in Medicine & Biology*, 56(17):5535–5552, 2011.
- [16] P Riviere and D Billmire. Reduction of noise-induced streak artifacts in x-ray computed tomography through penalized-likelihood sinogram smoothing. In *IEEE Transactions on Medical Imaging*, volume 24, pages 105–111, 2005.
- [17] K Suzuki, J Liu, A Zarshenas, T Higaki, W Fukumoto, and K Awai. Neural network convolution (nnc) for converting ultra-low-dose to virtual high-dose ct images. In *International Workshop on Machine Learning in Medical Imaging*, pages 334–343, 2017.
- [18] Z Tian, X Jia, K Yuan, T Pan, and S Jiang. Low-dose ct reconstruction via edge-preserving total variation regularization. *Physics in Medicine & Biology*, 56(18):5949–5967, 2011.
- [19] J. Wang, T. Li, and L. Xing. Iterative image reconstruction for cbct using edge-preserving prior. *Medical Physics*, 36(1):252–260, 2009.
- [20] Z Wang, A Bovik, H Sheikh, and E Simoncelli. Image quality assessment: from error visibility to structural similarity. *IEEE Transactions on Image Processing*, 13(4):600–612, 2004.
- [21] Q. Xie, D. Zeng, Q. Zhao, D. Meng, Z. Xu, Z. Liang, and J. Ma. Robust low-dose ct sinogram preprocessing via exploiting noise-generating mechanism. *IEEE Transactions on Medical Imaging*, 36(12):2487–2498, 2017.
- [22] J Xu and B Tsui. Electronic noise modeling in statistical iterative reconstruction. *IEEE Transactions on Image Processing*, 18(6):1228–1238, 2009.
- [23] Q Xu, H Yu, G Wang, and X Mou. *Low-Dose X-ray CT Reconstruction via Dictionary Learning*, volume 31. 2012.
- [24] Q Yang, P Yan, M Kalra, and G Wang. Ct image denoising with perceptive deep neural networks. *arxiv*, 2017.
- [25] X Yi and P Babyn. Sharpness-aware low-dose ct denoising using conditional generative adversarial network. *Journal of Digital Imaging*, pages 1–15, 2018.
- [26] Z Yin and J Shi. Geonet: Unsupervised learning of dense depth, optical flow and camera pose. *arxiv*, 2018.
- [27] D Zeng, J Huang, Z Bian, S Niu, H Zhang, Q Feng, Z Liang, and J Ma. A simple low-dose x-ray ct simulation from high-dose scan. *IEEE Transactions on Nuclear Science*, 62(5):2226–2233, 2015.
- [28] L Zhang, L Zhang, X Mou, and D Zhang. Fsim: a feature similarity index for image quality assessment. *IEEE Transactions on Image Processing*, 20(8):2378–2386, 2011.
- [29] M Zhu, S Wright, and T Chan. Duality-based algorithms for total-variation-regularized image restoration. *Computational Optimization & Applications*, 47(3):377–400, 2010.